




# Research on Vibration Control of FAST Feed Cabin Based on Active Mass Damper

Lucong Zhang<sup>1,2,3</sup> , Jinghai Sun<sup>1,3</sup>, and Peng Jiang<sup>1,3</sup>

<sup>1</sup> National Astronomical Observatories, Chinese Academy of Sciences, Beijing 100101, China; [lc Zhang@bao.ac.cn](mailto:lc Zhang@bao.ac.cn)

<sup>2</sup> University of Chinese Academy of Sciences, Beijing 100049, China

<sup>3</sup> Key Laboratory of Five-hundred-meter Aperture Spherical radio Telescope, Beijing 100020, China

Received 2024 August 17; revised 2024 September 26; accepted 2024 October 8; published 2024 November 6

## Abstract

In this paper, an effective active vibration control method was investigated to further improve the positioning accuracy of the Five-hundred-meter Aperture Spherical radio Telescope (FAST) feed cabin. The actual operation data of FAST was collected to analyze the vibration characteristics of the feed cabin in multiple directions. A simplified model of the cabin-cable system was established to evaluate the effects of a mass damper on different vibration frequencies and modes. On this basis, an active mass damper system and control system were designed for the cabin with multiple degrees of freedom and modal variation characteristics. Theoretical calculation and simulation proved that it has a significant effect on improving the damping of the cabin-cable system and suppressing the vibration of the FAST feed cabin.

**Key words:** telescopes – methods: data analysis – instrumentation: miscellaneous – techniques: miscellaneous – Astronomical Instrumentation – Methods and Techniques

## 1. Introduction

The Five-hundred-meter Aperture Spherical radio Telescope (FAST) is the largest and most sensitive single-aperture radio telescope (Figure 1). Since its opening in 2020, FAST has maintained stable and efficient operation, and has achieved a number of important detections on a series of scientific targets such as pulsars, fast radio bursts, neutral hydrogen, etc. Meanwhile, the engineering team has also been exploring in several technical directions to enhance the telescope's competitiveness in frontier astronomical exploration. For example, through the development of new receivers to improve the efficiency of sky survey and expand the range of observation frequencies, and through the application of new measurement and control technologies to improve the observing sensitivity and pointing accuracy.

The FAST feed cabin (Figure 2) is suspended by six long-span parallel cables. The cable system has complex dynamics and is susceptible to pulsating wind disturbances in the environment. Precise positioning of the feed inside the cabin is achieved by three-stage series control. First, the feed cabin is towed by the six cables, and the accuracy of position and attitude of the cabin is initially controlled within 48 mm and 1°, respectively. Second, the AB-axis mechanism, which can rotate around two orthogonal axes in the cabin, is used to compensate the deviation between the feed's attitude under the optimized state of the cable force and the expected attitude during observation. Finally, the Stewart platform in the cabin compensates for the residual error in real time, so as to keep

the positioning accuracy of the feed at a level better than the rms of 10 mm (Nan 2006; Tang et al. 2011; Jiang et al. 2019, 2020). The current feed control scheme has fully considered the dynamic characteristics of the adjustment mechanisms at all levels, and has effectively avoided the resonance risk of multi-stage control of flexible structure by restricting the control bandwidth, so that the telescope has achieved the expected observational sensitivity and pointing accuracy in the  $L/S$  band (Qian et al. 2020).

From the analysis of FAST's actual operation data, it is known that the residual positioning error of the feed mainly came from the vibration of the feed cabin caused by the large span cables. Therefore, the suppression of the cabin vibration has become a new approach to further improve the positioning accuracy of the feed. Under the existing feed support scheme, it is difficult to restrain vibration by adjusting the structure parameter itself, so additional vibration control equipment needs to be considered. By increasing the damping of the cabin-cable system, not only the vibration on each modal frequency can be directly reduced, but also the response bandwidth of the original closed-loop controller can be increased to further increase the positioning accuracy.

Mass dampers are widely used in engineering, which are generally categorized as tuned mass damper (TMD), active mass damper (AMD) and semi-active tuned mass damper (SATMD). The mass damper is connected as a substructure to the main structure where vibration suppression is required. TMD (Figure 3(a)) relies on mechanical springs and dampers to



**Figure 1.** The aerial view photograph of FAST.

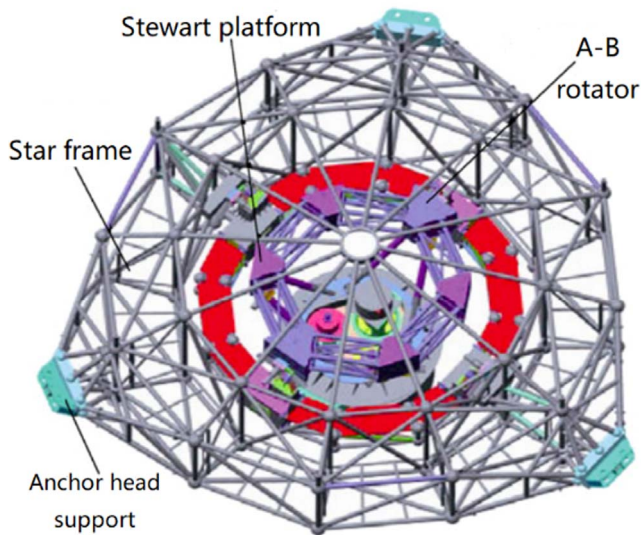


**Figure 2.** Schematic diagram of FAST feed cabin structure.

suppress a certain mode of vibration. AMD (Figure 3(b)) generates force through the driving mechanism according to the actual vibration of the main structure, therefore a wide range of vibration modes can be suppressed. SATMD (Figure 3(c)) is mainly passive, but the damping and stiffness of the substructure can be adjusted in a limited range, resulting in different forces to adapt the variation of vibration frequency.

Specific to the application of the FAST feed cabin, there are the following characteristics:

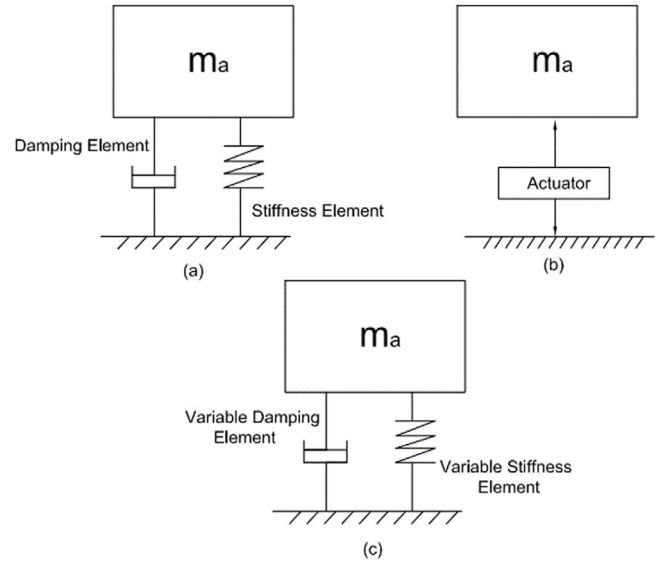


**Figure 3.** Category of Mass Damper (a) Tuned mass damper(TMD)/ (b) Active mass damper(AMD)/ (c) Semi-active tuned mass damper(SATMD).



**Figure 4.** The working environment of FAST feed cabin.

1. The vibration of the feed cabin is a compound motion with six degrees of freedom in space.

2. The workspace of the feed cabin is a spherical cap located about 140 m above the bottom of the reflector, with an aperture of more than 200 m (Figure 4). As the position of the feed cabin changes, the length and shape of the cable network varies, leading to constant changes in the vibration modes and frequencies.

3. The natural frequencies of the cabin-cable system are very low, mainly concentrated below 1 Hz, and the first-order resonance frequency is even below 0.2 Hz.

The vibration modes are complex and the frequencies are constantly changing, making a TMD have very slight effects in

most of the working time. Due to the low vibration frequencies, any form of mass damper with a spring element would make it difficult to maintain the equilibrium position of the mass block. Therefore, an AMD is the best choice due to its active actuation to adapt to changes and maintain the equilibrium of the mass block.

Lefteris Koutsoloukas and Nikolaos Nikitas (Koutsoloukas et al. 2022) summarized 208 application cases of mass dampers on large buildings or facilities, of which AMDs accounted for 4%. The difficulties in the application of AMD lay in the need for external energy to generate driving force, and in order to achieve a good vibration suppression effect, it was necessary to maintain stability and reduce the time lag of the control system, which increased the cost of the application. However, under perfect application conditions, the AMD could adapt to a variety of disturbances and responses, had strong robustness and flexibility, and could realize an optimal control effect by choosing appropriate control algorithms when facing different control objectives.

In the vibration suppression study of the FAST feed support system, Su and Duan designed an electrorheological fluid damper for the fluctuating wind vibration of the cables (Su et al. 2003). The damper was installed on a long section of the suspension cable near the cabin, and the voltage of the electrorheological fluid damper was controlled by the wind speed measuring device to counteract the wind disturbance. The damper could reduce the vibration of the cable in specific modes, thus reducing the vibration of the cabin indirectly. However, the configuration and dynamic changes of the cabin-cable system were not involved, therefore the effectiveness of the damper in a complex and changing operating environment could not be analyzed and verified.

In order to suppress the feed cabin's vibration around the first-order resonant frequencies, Dong and Duan designed a set of multi-tuned mass dampers installed on the feed cabin (Dong et al. 2002). The main purpose of these dampers was to suppress the interference of pulsating winds. Each mass damper only suppressed the horizontal vibration in a specific mode, and cannot cope with the frequency changing during operation. Furthermore, hanging more TMDs would inevitably increase the mass of the cabin.

In this paper, the vibration in certain directions which can significantly affect the quality of observations is first determined by collecting and analyzing the actual operating data of FAST. On this basis, an AMD system suitable for multi-degree-of-freedom and frequency variation characteristics of the feed cabin is designed. Finally, its effect on improving the damping of the cabin-cable system and suppressing the vibration of the feed cabin is verified by the theoretical calculation and simulation analysis.

**Table 1**  
The Contents of Selected Data Set

Name	Unit	Description
$t$	s	Recording time
$(x, y, z)_p$	m	Planned position of the centroid of the feed cabin
$(x, y, z)_A$	m	Actual position of the centroid of the feed cabin
$(\text{Yaw, Pitch, Roll})_p$	rad	Planned attitude angle of feed cabin
$(\text{Yaw, Pitch, Roll})_A$	rad	Actual attitude angle of feed cabin

## 2. Vibration Data Analysis

The feed cabin has different trajectories and positions in different observation cases, but the vibration in each case has similar characteristics. Therefore, a typical set of operating data is selected, and the vibration data is extracted and transformed from the global coordinates of the telescope to the local coordinates of the cabin. On this basis, the vibration can be decomposed into the primary optical axis direction, by which the influence on astronomical observation can be determined. This paper analyses an observation record of FAST in tracking mode on 2022 September 22. The tracking lasted about 1500 s. The data set contains the entire motion information of the feed cabin in time series (Table 1), including the feed cabin's planned position and actual position in the global coordinate system of the telescope, as well as the planned attitude angle and actual attitude angle of turning around along the axis in the local coordinate system of the feed cabin.

As shown in Figure 5, the global coordinate system of FAST is defined with the spherical center of the active reflector as the origin, the north direction as the X-axis, the east direction as the Y-axis, and the zenith direction as the Z-axis. There are two local coordinate systems in the feed cabin as shown in Figure 6. The first one is fixed on the feed cabin. The mass center of the cabin is the origin, and the Z-axis points to the top of the cabin, X and Y-axis directions are determined according to the right-hand rule. The rotation angles along the X, Y and Z axes of the local coordinate system are defined as Roll, Pitch and Yaw angles, respectively. Another one is fixed on the phase center of the feed and is parallel with the first one in the initial state.

During observations, there are two more important directions should be defined. As shown in Figure 5, the primary optical axis is defined as a straight line through the phase center of the feed and the spherical center of the active reflector, which indicates the direction of the telescope's pointing. The focal plane is perpendicular to the primary optical axis and passing through the phase center of the feed. Therefore, the vibration of the feed cabin can be decomposed from the global coordinates to this axial plane combination to analyze the influence on the telescope's pointing.

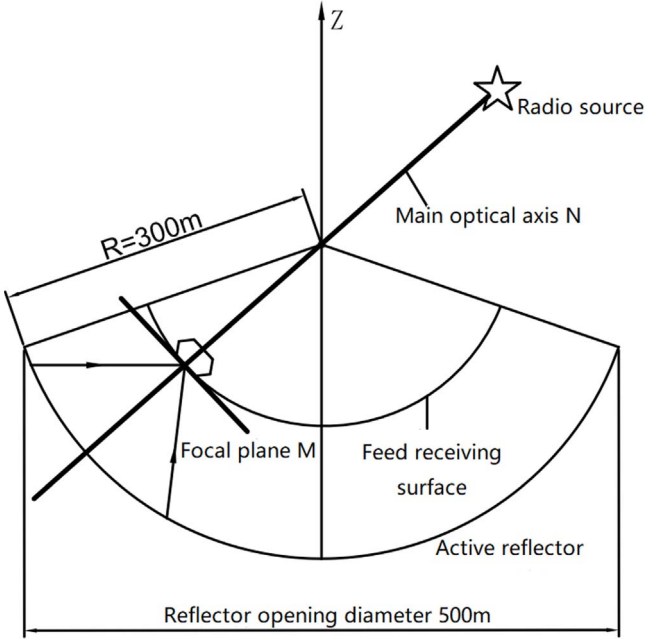


Figure 5. The global coordinate system of FAST.

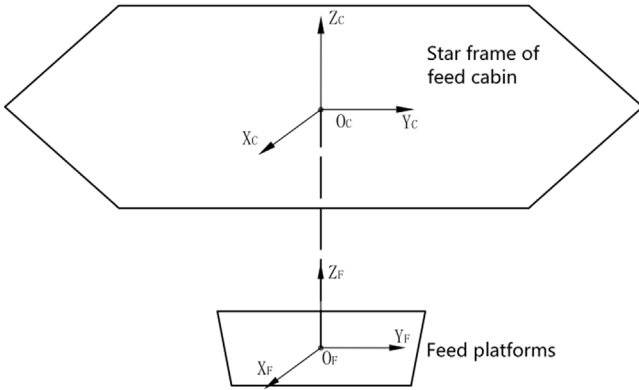


Figure 6. The local coordinate system of the feed cabin.

As shown in Figure 7, the translation error of the feed cabin can be derived by calculating the difference between the theoretical and actual coordinates in the global coordinate system.

The phase center of the feed is not in the centroid of the feed cabin, the attitude error of the feed cabin will pass on to the receiver feed to produce position deviation. When the attitude angle of the cabin changes, the rotation error around the Z-axis in the local coordinate system is less than  $10^{-6}$  rad, which will not affect the observation and is ignored in the analysis. In the analysis of the rotation error, only the error caused by the rotation of Pitch and Roll angles is considered.

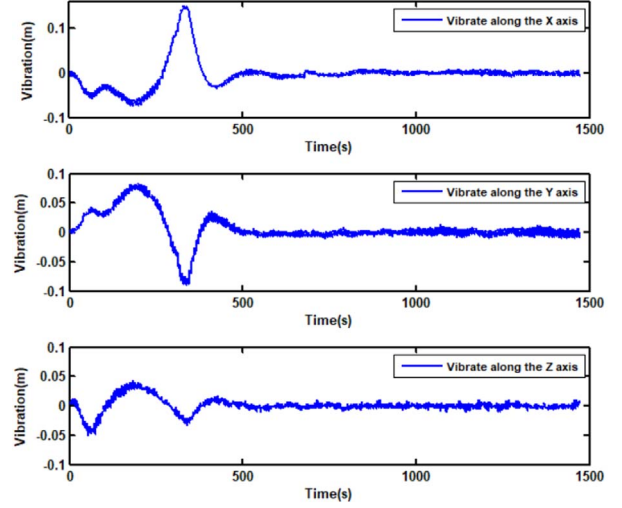


Figure 7. Translation error of platform on feed cabin.

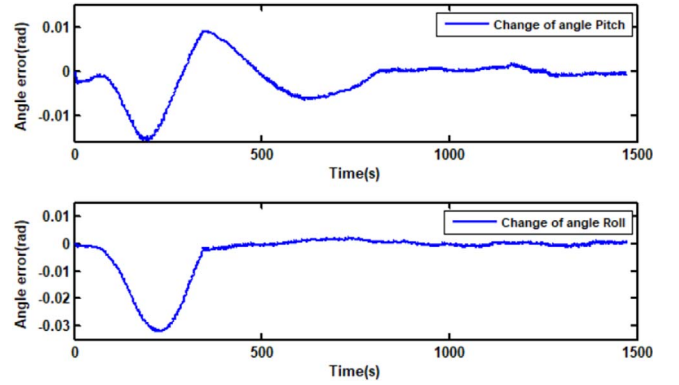


Figure 8. Angle error of feed cabin.

The rotation error is obtained by the difference between the planned coordinates of the attitude angle and the actual coordinates as shown in the figure:

As shown in Figures 7 and 8, in the initial 600 s of operation, the system is entering the tracking observation from the high-speed source changing, the large inertia of cabin-cable system and the integral controller caused oscillation, and the oscillation needed more time to be suppressed by the controller, so the data after 1000 s is selected as the cabin is in a smooth tracking status, to analyze the vibration caused by the cabin-cable dynamics.

### 2.1. Translational Error

The feed cabin can be treated as a rigid body relative to the long-span cables. Its translation will be directly transferred to the feed in the cabin, which is one of the main sources of feed



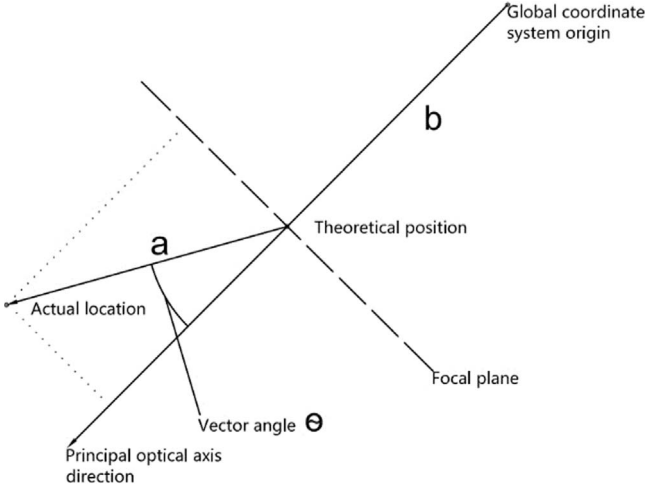


Figure 9. Translational error decomposition.

positioning errors. In order to further analyze the influence of translational error on the observation accuracy of FAST, the translational error should be decomposed from the global coordinate system to the focal plane and primary optical axis in the local coordinate system.

As shown in Figure 9, the spatial error vector of the feed's phase center (a) is from the theoretical position to the actual position, and the primary optical axis vector (b) is from the origin of the global coordinate system to the theoretical position. The angle between the spatial error vector and the primary optical axis is  $\theta$ , which can be obtained by using the vector angle formula.

The length of the spatial error vector can be calculated by

$$L = \sqrt{(x_A - x_P)^2 + (y_A - y_P)^2 + (z_A - z_P)^2}, \quad (1)$$

The component along the primary optical axis is

$$l_z = L \cos(\theta), \quad (2)$$

and the component in the focal plane is

$$l_j = L \sin(\theta). \quad (3)$$

Therefore the translation error is decomposed on the primary optical axis and focal plane as shown in Figure 10:

## 2.2. Rotational Error

The attitude error of the feed cabin will also be transmitted to the feed to bring additional displacement. Therefore, it is necessary to analyze the influence of rotational error on observation accuracy and observation range. Due to the small angle, the radian of the receiver platform rotation can be approximated as a linear displacement, which can also be called an angular displacement. Following the previous

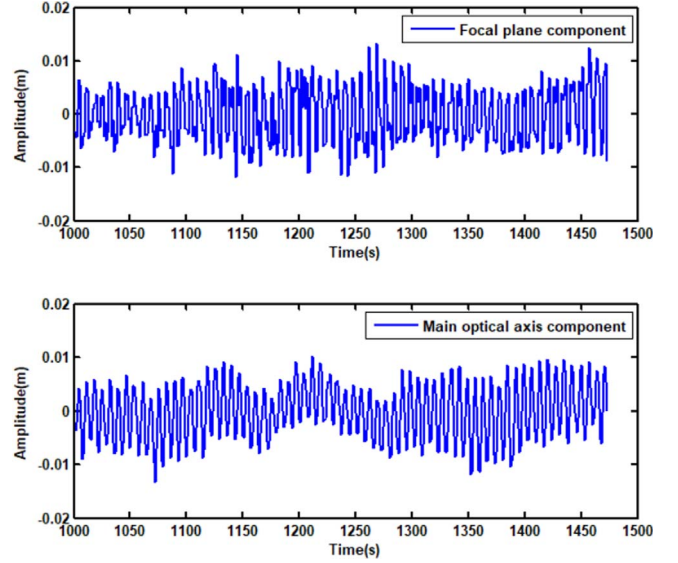


Figure 10. Translation error in local coordinate system.

definition of attitude angle, the total angular displacement error  $L_1$  caused by the angle error around the  $X$  and  $Y$  axes can be calculated through the formula:

$$L_1 = \sqrt{(\Delta \text{Pitch} \cdot l)^2 + (\Delta \text{Roll} \cdot l)^2}. \quad (4)$$

In Equation (4),  $l$  is the distance between the two local coordinate system's origin (from the mass center of the cabin to the phase center of the feed), with a value of 1.75 m.  $\Delta \text{Pitch}$  and  $\Delta \text{Roll}$  is the difference between the planned and actual attitude angles of the feed cabin. The angular displacement error caused by rotation around each axis and the total angular displacement error synthesized by the vector is shown in Figure 11:

The steady-state error of the total angular displacement error is first eliminated by the Fourier transform. Then the total angular displacement error is decomposed toward the primary optical axis and the focal plane as shown in Figure 12.

The mass center of the cabin ( $O_C$ ) is connected to the phase center of the feed by a virtual connecting rod, the length ( $l$ ) of the connecting rod is 1.75 m.  $F_1$  represents the feed's planned position and  $F_2$  represents the feed's actual position,  $L_1$  is the distance between  $F_1$  and  $F_2$ , which is given by Equation (4). The angular displacement is decomposed to the primary optical axis and the focal plane, and the angle between the vector of the actual position pointing to the theoretical position and the focal plane is  $c$ . From the relationship in the diagram, it can be seen that the angle  $c$  is half of the angle between  $F_1$  and  $F_2$ :

$$c = \arcsin\left(\frac{0.5 \cdot L_1}{l}\right), \quad (5)$$

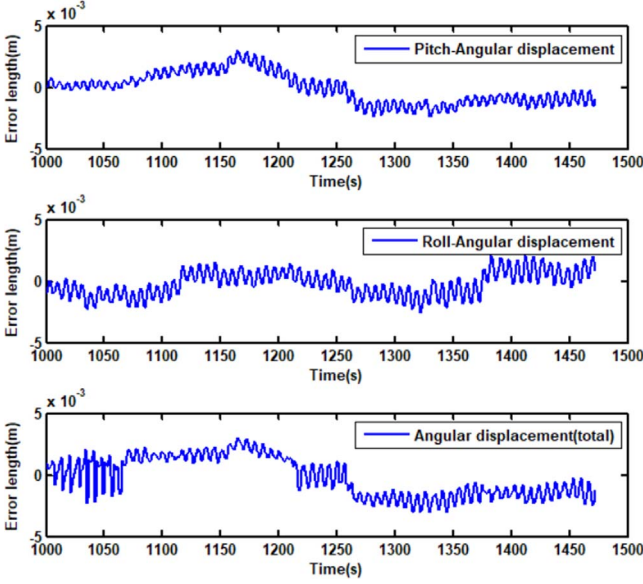


Figure 11. Displacement error caused by cabin rotation.

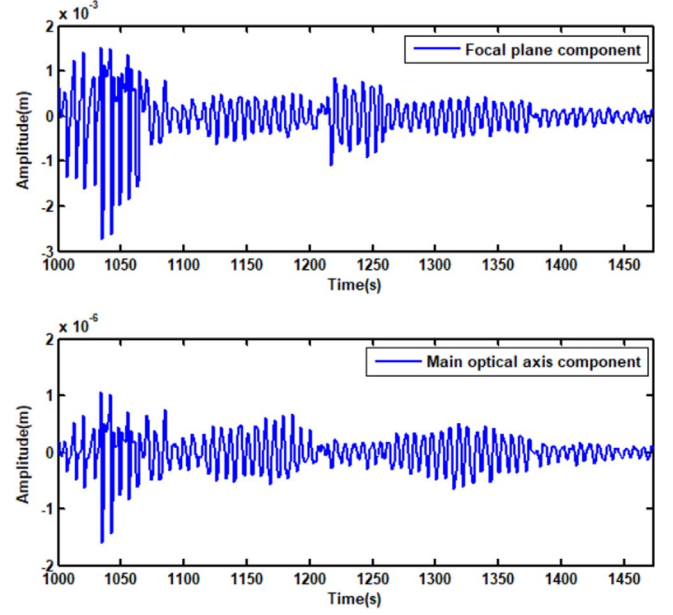


Figure 13. Angular displacement error in local coordinate system.

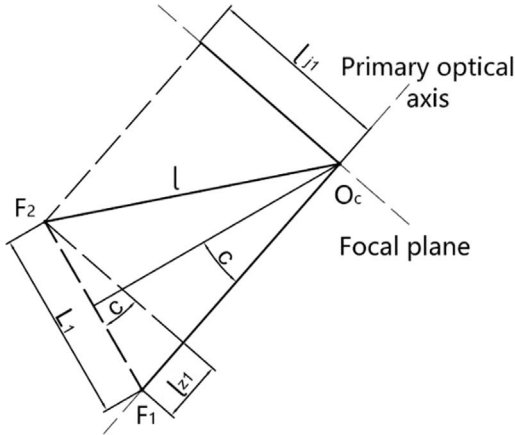


Figure 12. Angular displacement decomposition.

Furthermore, the component  $l_{z1}$  of the angular displacement on the primary optical axis can be obtained as

$$l_{z1} = L_1 \cdot \sin(c), \quad (6)$$

and the component  $l_{j1}$  of angular displacement on the focal plane is

$$l_{j1} = L_1 \cdot \cos(c). \quad (7)$$

The decomposed angular displacement is shown in Figure 13:

**Table 2**  
Comparison of the Error's Maximum Amplitude

Data Name	Max
Primary optical axis component of angular displacement error	$8.9 \times 10^{-5}$
Focal plane component of angular displacement error	0.124
Primary optical axis component of translational error	1.473
Focal plane component of translational error	1.305

### 2.3. Frequency Domain Analysis

In order to compare the influence of translation error and angular displacement error on the main vibration frequency, the errors decomposed on the primary optical axis and focal plane are transformed to the frequency domain. After removing the steady-state error of the data, the images are shown in Figure 14, and the maximum amplitudes are listed in Table 2.

As shown in Table 2, the maximum values of the feed positioning error in two directions are 1.473 mm and 1.305 mm, both are caused by the translation error. The two directions have comparable values, which are the main sources of error. The angular displacement error also affects the feed positioning error, mainly in the direction of the focal plane.

### 3. Mass Damper Scheme

According to the error analysis of the above three sections, the following conclusions can be synthesized:

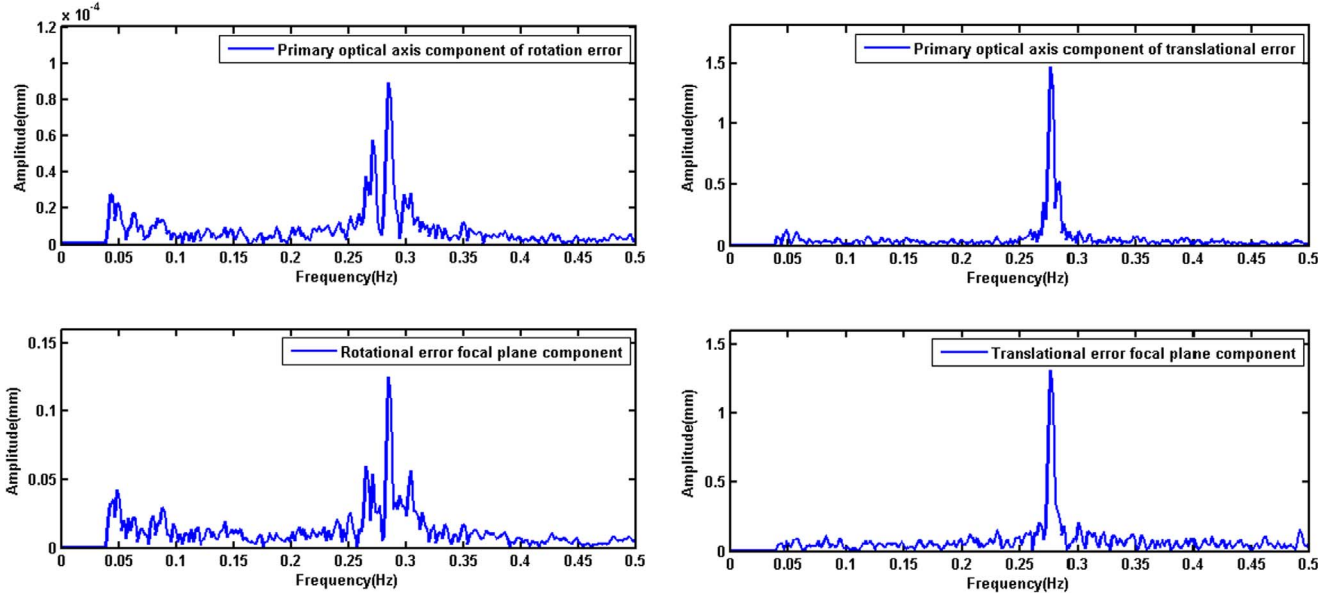


Figure 14. The decomposed error component in the frequency domain.

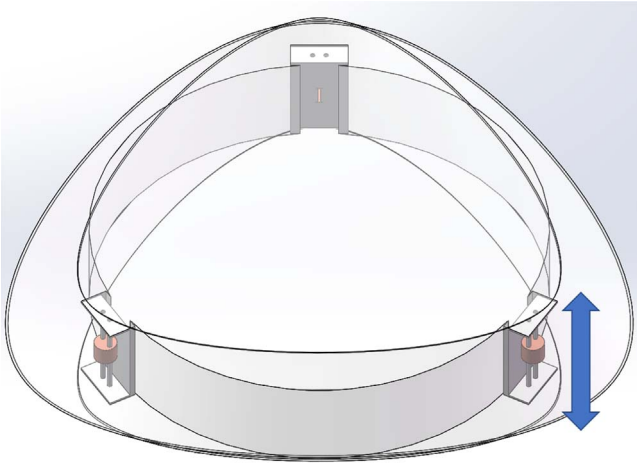


Figure 15. Damper system layout.

- (1) Both the translational error and angular displacement error have influence on the feed cabin's observation accuracy, but the feed is more affected by the translational vibration error. The suppression effect of the AMD on the translational error is the key to test its effectiveness.
- (2) A single mass damper with multiple degrees of freedom is highly complex and hard to achieve. Therefore the multi-direction of vibration determines that the number and position of AMDs should not be single.

- (3) Due to space and weight constraints of the cabin, the AMD cannot be installed along both the focal plane and the primary optical axis direction.

After weighing the advantages and disadvantages, the optimum solution is to distribute three sets of AMDs spaced  $120^\circ$  apart at the maximum diameter of the cabin's outside edge. As shown in Figure 15, the masses move along a guide parallel to the primary optical axis. The movement of the masses is controlled by a linear drive mechanism, eliminating the need for mechanical springs and additional dampers. This not only simplifies the structure and saves space, but also improves stability. This design can directly and effectively suppress translation errors in the direction of the primary optical axis and minimize angular displacement errors caused by the rotation of the cabin. Since the cabin is a compound motion, vibration in the focal plane will also be suppressed to a certain range after the mass damper is installed to increase system damping.

#### 4. Effect Analysis of Mass Damper in Feed Cabin

To analyze the vibration-suppressing capability of the damper and to preliminarily determine the reasonable parameter of the damper, a simplified multi-DoF model of the cabin-cable system is established, and an AMD is set up on this model. The overall model is shown in Figure 16, in which  $m_1$  is  $15t$ , representing the mass of long-span cable,  $m_2$  is  $30t$ , representing the mass of the cabin,  $m_a$  is the mass of damper, the value is  $1/10$  of the cabin, which is  $3t$ . The first-order

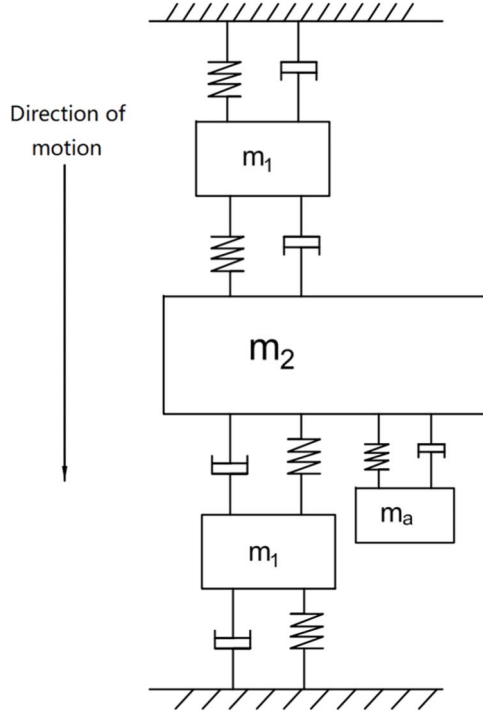


Figure 16. The simplified multi-DoF model of FAST cabin-cable system.

natural frequency of the FAST feed cabin support system is 0.18 Hz and the damping ratio is 0.002. The stiffness and damping factor of the system are  $50,000 \text{ N m}^{-1}$  and 500, respectively. First of all, based on the force analysis of three mass blocks, the three displacements are merged into a vector

$$q = \begin{bmatrix} x_1 \\ x_2 \\ x_3 \end{bmatrix}.$$

Therefore the dynamic equation of the system without the AMD is established as

$$\begin{bmatrix} m_1 & 0 & 0 \\ 0 & m_2 & 0 \\ 0 & 0 & m_1 \end{bmatrix} \ddot{q} + \begin{bmatrix} 2c & -c & 0 \\ -c & 2c & -c \\ 0 & -c & 2c \end{bmatrix} \dot{q} + \begin{bmatrix} 2k & -k & 0 \\ -k & 2k & -k \\ 0 & -k & 2k \end{bmatrix} q = \begin{bmatrix} f_1 \\ 0 \\ 0 \end{bmatrix}. \quad (8)$$

$f$  is the external force applied on each mass. The first-order and second-order undamped natural frequencies of the model can be calculated by solving the characteristic equations of the above equation, which are 0.18 and 0.42 Hz respectively. The first-order damping ratio is 0.002, and the second-order damping ratio is 0.005, which is equivalent to that of the FAST prototype.

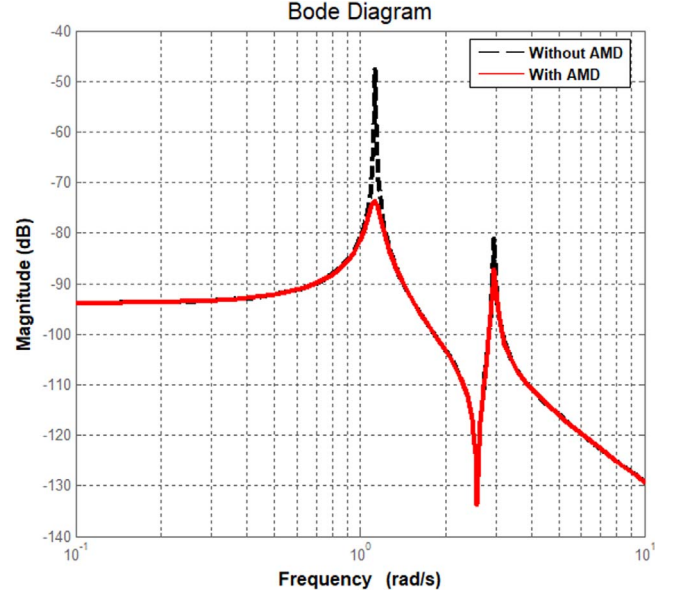


Figure 17. System response with/without an AMD.

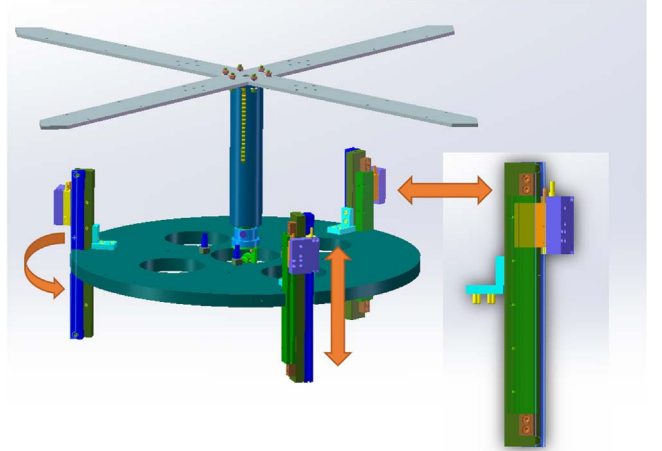


Figure 18. Simplified vibration platform for feed cabin.

Table 3  
Main Parameters of the Vibration Platform

Parameter	Data	Parameter	Data
Cabin diameter	800 mm	Stiffness of main spring	$K = 1236 \text{ N m}^{-1}$
Cabin thickness	30 mm	Moment of inertia	$\begin{bmatrix} 1.634 & 0 & 0 \\ 0 & 3.262 & 0 \\ 0 & 0 & 1.634 \end{bmatrix}$
First-order natural frequency	0.34 Hz	Mass block quality	1 Kg
Second-order natural frequency	0.83 Hz	Cabin mass	40.8 kg



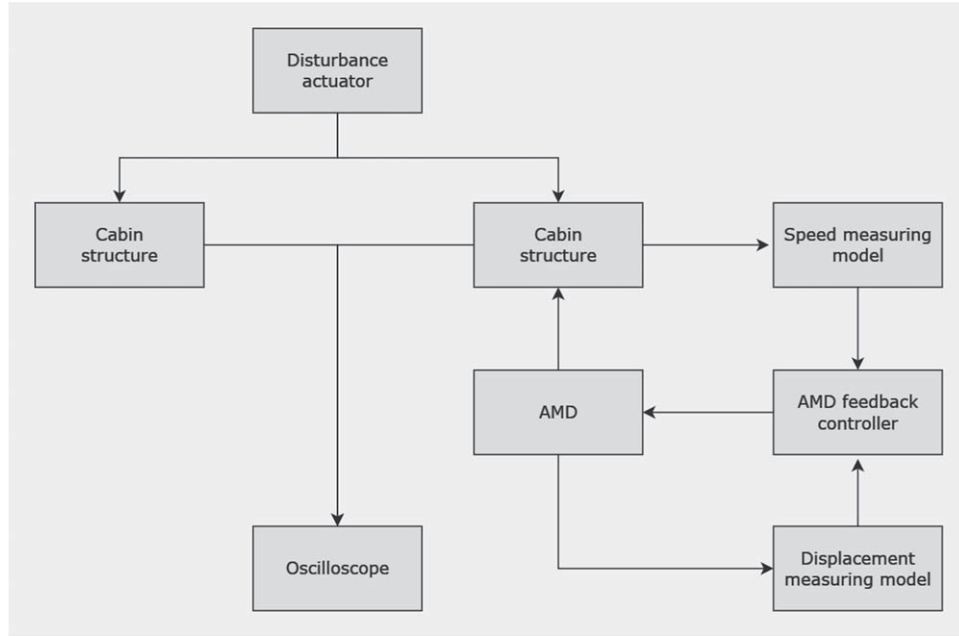


Figure 19. Operation flow chart of the simulation.

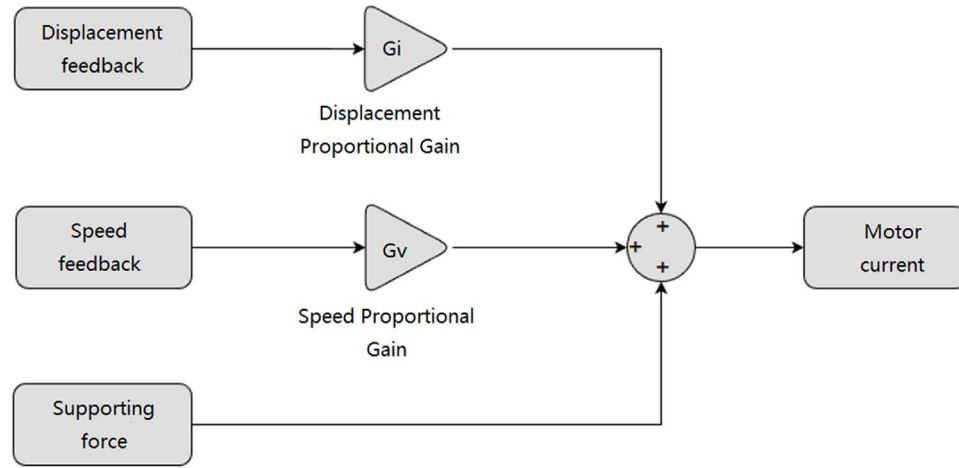
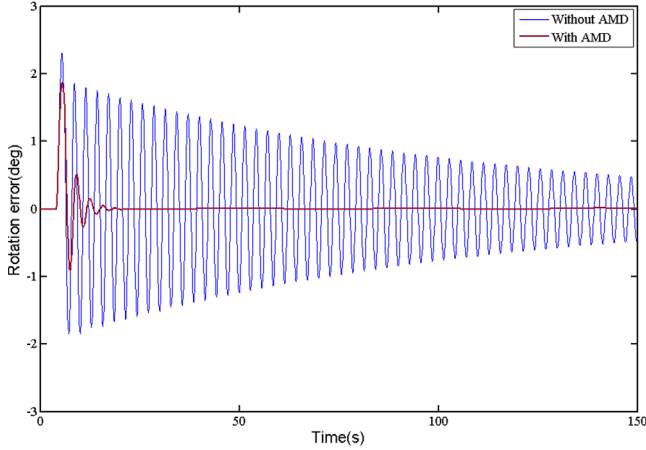


Figure 20. Feedback controller schematic diagram.

**Table 4**  
Error Comparison Under the Action of Variable Force

Error Type	Tracking	Swift Calibration	Snap Shotdec	On The Fly Mapping
Vibration error (m)	0.0078	0.0063	0.0072	0.0105
Vibration error (AMD) (m)	0.0046	0.0032	0.0027	0.0038
Rotational error (deg)	1.0462	0.9271	1.02	1.577
Rotational error (AMD) (deg)	0.4842	0.4128	0.3661	0.5621
Overall error (m)	0.0328	0.029	0.032	0.0493
Overall error (AMD) (m)	0.0154	0.013	0.0115	0.0176



**Figure 21.** Comparison of rotational errors under pulse disturbance.

In order to verify the effect of AMD with velocity feedback, the system dynamics equation after adding AMD is established as

$$M_1 \ddot{q} + D_1 \dot{q} + K_1 q = f \quad (9)$$

where

$$q = \begin{bmatrix} x_1 \\ x_2 \\ x_3 \\ x_a \end{bmatrix},$$

$$M_1 = \begin{bmatrix} m_1 & 0 & 0 & 0 \\ 0 & m_2 & 0 & 0 \\ 0 & 0 & m_1 & 0 \\ 0 & 0 & 0 & m_a \end{bmatrix},$$

$$D_1 = \begin{bmatrix} 2c & -c & 0 & 0 \\ -c & 2c + c_a + G_v & -c & -c_a \\ 0 & -c & 2c & 0 \\ 0 & -c_a - G_v & 0 & c_a \end{bmatrix},$$

$$K_1 = \begin{bmatrix} 2k & -k & 0 & 0 \\ -k & 2k + k_a & -k & -k_a \\ 0 & -k & 2k & 0 \\ 0 & -k_a & 0 & k_a \end{bmatrix},$$

and

$$f = \begin{bmatrix} f_1 & 0 & 0 & 0 \\ 0 & f_2 & 0 & 0 \\ 0 & 0 & f_3 & 0 \\ 0 & 0 & 0 & 0 \end{bmatrix}.$$

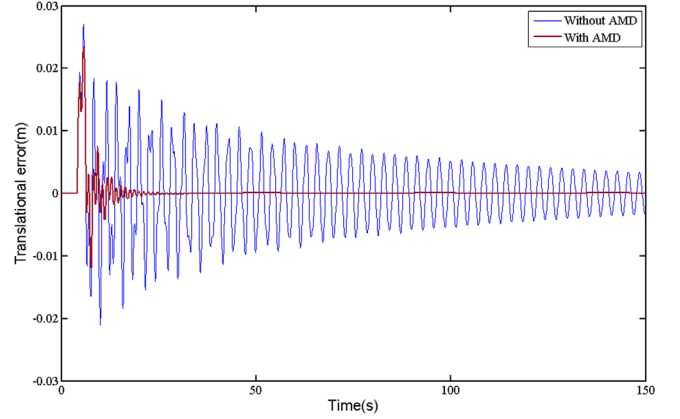


**Figure 22.** Comparison of translational errors under pulse disturbance.

To analyze the system response, the equation is transformed into the form of state space equation

$$\begin{bmatrix} \dot{q} \\ \ddot{q} \end{bmatrix} = \begin{bmatrix} 0 & I \\ -M^{-1}K & -M^{-1}D \end{bmatrix} \begin{bmatrix} q \\ \dot{q} \end{bmatrix} + \begin{bmatrix} 0 \\ M^{-1} \end{bmatrix} f$$

$$\begin{bmatrix} q \\ \dot{q} \end{bmatrix} = \begin{bmatrix} I & 0 \\ 0 & I \end{bmatrix} \begin{bmatrix} q \\ \dot{q} \end{bmatrix} + \begin{bmatrix} 0 \\ 0 \\ M^{-1} \end{bmatrix} f \quad (10)$$

where  $G_v$  is the velocity feedback gain,  $k_a$  is the elastic coefficient and  $c_a$  is the damping coefficient of AMD. In this paper, the AMD design only depends on the linear drive mechanism to control the motion of the mass block, so the values of  $c_a$  and  $k_a$  are 0, and the velocity feedback gain  $G_v = 500$ .

The comparison of the system response between the original system and the system equipped with a velocity feedback AMD is shown in Figure 17.

When velocity feedback is used, the first-order damping ratio is 0.0451 and the second-order damping ratio is 0.0121. For comparison, the first-order damping ratio is about 19 times higher, and the first-order damping ratio is about 2 times higher than that of the original system.

The above results show that the AMD with velocity feedback is effective. AMD can improve the first-order and second-order damping ratio of the feed cabin, which can make the cabin reach a steady-state as soon as possible.

## 5. Design and Simulation of the Vibration Platform for Feed Cabin

To further verify the vibration-suppressing effect of the mass damper system on multiple vibration directions of the feed cabin, an indoor simplified vibration platform is designed

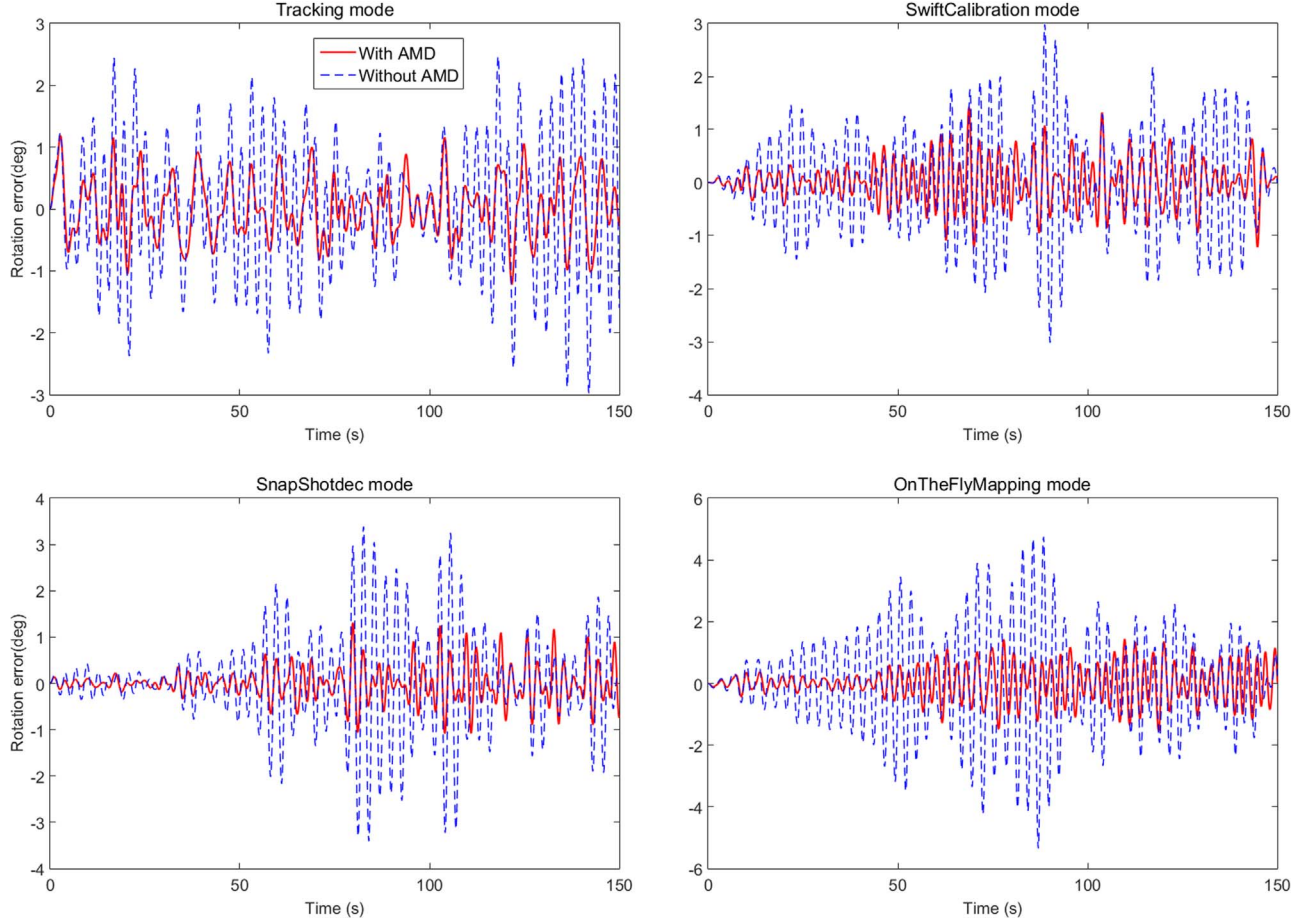


**Figure 23.** Comparison of rotation errors under complex disturbance.

(Figure 18). The purpose of designing the AMD in this paper is to restrain the feed cabin's translation in the direction of the primary optical axis and the rotation around the  $X$  and  $Y$  axes. In order to simplify the vibration mode of the feed cabin, a rigid bracing mechanism with three degrees of freedom is designed to replace the prototype cable-cabin structure. The support mechanism uses a Hooke's hinge to constrain the feed cabin's rotation along the horizontal axis. The center of mass of the feed cabin is adjusted slightly below the Hooke's hinge, so that the cabin is able to vibrate freely in the manner of a single pendulum. The Hooke's hinge is connected to the support structure with a spring so that the cabin is able to vibrate in the vertical direction. The main parameters of the vibration platform are shown in Table 3.

The frequency of the vertical translation of the feed cabin can be adjusted by adjusting the spring stiffness. The rotation frequency of the feed cabin along the horizontal axis can be adjusted by adjusting the distance between the center of the Hook hinge and the center of mass of the feed cabin.

### 5.1. Simulation Model of Vibration Platform for Feed Cabin

In order to investigate the required parameters and vibration suppression effect of AMDs on the vibration platform of the feed cabin, a simulation was carried out before performing the physical modeling experiments. The SimMechanics toolkit in MATLAB/SIMULINK environment was used to build the simulation model of the whole system. Its operation flow chart is shown in Figure 19.

The whole simulation model includes the feed cabin platform without mass damper and the cabin platform with AMD. In the second part, the cabin platform is attached by an AMD module, as well as two measurement modules and AMD feedback controller.

The parameters of the two feed cabins are exactly the same to compare the vibration before and after the installation of AMDs. The mass damper model consists of three mass blocks connected to the cabin platform through a linear driver.

Two measurement modules are set up in the simulation model to provide feedback signals to the damper's controller.

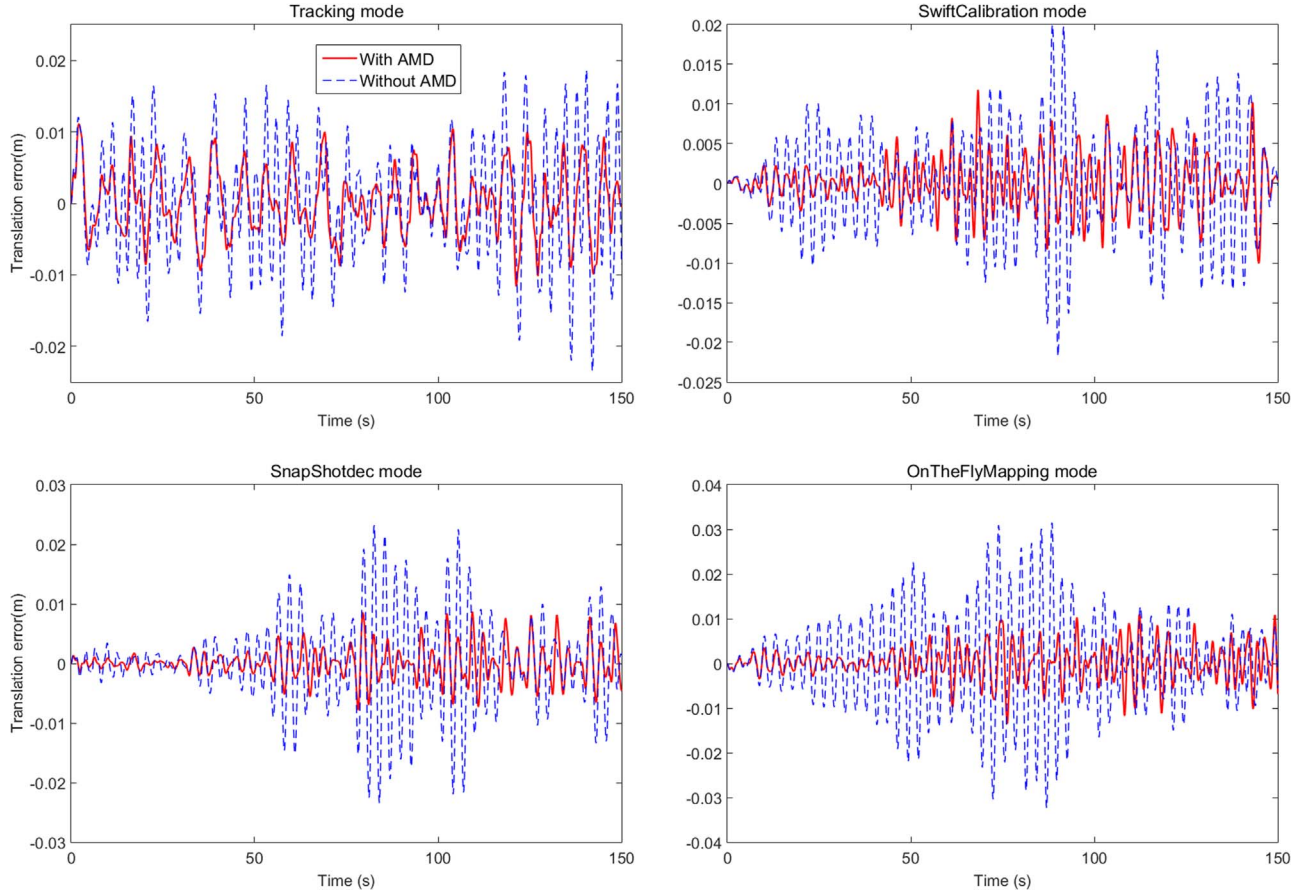


**Figure 24.** Comparison of translational errors under complex disturbance.

The velocity measurement module is used to output the vibration speed of the platform, and the displacement measurement module outputs the displacement of the mass block of the damper relative to the cabin platform.

As shown in Figure 20, the feedback controller calculates the driving force applied to the mass block according to the feedback signal. The feedback gain coefficient is determined according to the maximum amplitude of the vibration and the maximum moving range of the mass. The maximum length of the mass guide in the simulation model is 300 mm, so the travel feedback gain is required to restrict the displacement of the mass block within 300 mm. Under the condition that the displacement of the mass block is satisfied, the larger the velocity feedback gain is, the faster the vibration platform returns to a steady-state. Here the displacement feedback gain is  $-0.05$  and the speed feedback gain is  $5$ .

Through the disturbance generator, the excitation is generated to make the vibration platform model of the feed cabin, which is equivalent to the actual amplitude of the cabin. With and without AMD, the angular error of the cabin and the translational error in the direction of the primary optical axis are output, respectively, to visually verify the effect of AMD.

## 5.2. The Simulation Result

First of all, an impulse disturbance of the same amplitude is input to the model group. With or without AMD, the simulation results of the feed cabin's rotational error and translation error in the direction of the primary optical axis are shown in Figures 21 and 22.

Then, a set of actual disturbance forces in the four different operating modes "Tracking," "SwiftCalibration," "SnapShotdec," and "OnTheFlyMapping" up to 150 s long is solved by inverse dynamics from the observation record data, and input to disturbance actuator to simulate the pulsating wind interference in the environment. The force components include the force on the cabin in the direction of the primary optical axis and the force that rotates the cabin around the  $X$  and  $Y$  axes. With and without AMD, the simulation results of the cabin's two kinds of errors in the direction of the primary optical axis are shown in Figures 23 and 24.

Calculating the rms value of the error signal with and without AMD on the platform, the list is shown in Table 4.

From Figures 21 and 22, it can be seen that under impulse interference, the vibration decay time of the AMD-equipped



cabin model is significantly reduced. While relying on the lower damping ratio, it takes about 400 s for the original system to reduce the vibration to less than  $10^{-4}$  m. The system with AMD takes less than 90% time to reduce the vibration error to less than  $10^{-4}$  m. Combining four different operation modes, under the disturbing forces solved by the inverse dynamics, the AMD-equipped system reduces the translational error by 55% and the rotational error by 60% compared to the original system. The angular displacement error can be obtained from the rotational error, and then the overall error can be obtained by combining the translational and rotational errors in orthogonal directions. The AMD-equipped system reduces the translational error by 59% compared to the original system. From the simulation results, it can be seen that the AMD significantly reduces the translational and rotational errors on the primary optical axis, which verifies the effectiveness of the AMD.

## 6. Conclusions

In this paper, we analyzed the operating data of the FAST feed cabin. Through the quantitative comparison of the translational error and the rotational error on the local coordinate system of the feed cabin, it is determined that the cabin is more affected by the translational error. Combined with the working environment of the feed cabin, a mass damper system including three AMDs are designed, spaced at  $120^\circ$  apart at the maximum diameter of the cabin's outside edge.

A simplified cabin-cable system model with three degrees of freedom is established, and an AMD is installed on it to analyze the vibration suppression ability of the damper. The analysis results show that the velocity feedback can significantly restrain the low-frequency vibration of the cabin.

A simplified simulation model of the feed cabin vibration platform is established to analyze the vibration suppression effect of the mass damper system in multiple vibration

directions of the feed cabin. The results show that the AMD has a significant suppression effect on the vibration in the direction of the primary optical axis and the rotation error around the  $X$  and  $Y$  axes caused by pulsating wind. After AMD assembly, the time to restore stability is reduced to about 10% of the original system. When facing the continuous interference force, AMD can also reduce the translational error in the direction of the primary optical axis to 45% of the original system, and the rotational error around the  $X$  and  $Y$  axes to 40% of the original system. Overall error was reduced to 41% of the original system. The simulation experiments have successfully verified the effectiveness of AMD.

This paper also provides a reference for the design of the FAST 2nd generation feed cabin, which will add the installation space of AMD with weight reduction. Looking forward, we will continue to research and design the AMD which has a better suppression effect. On the basis of the existing design, the active variable gain mechanism of the AMD control system (Nagashima 1997) will be added to solve the contradiction between the stroke limitation of the mass block and the vibration suppression effect.

## ORCID iDs

Lucong Zhang  <https://orcid.org/0009-0008-4221-4353>

## References

- Dong, Z. Q., Duan, B. Y., & Qiu, Y. Y. 2002, *JAM*, 03, 116
- Jiang, P., Tang, N.-Y., Hou, L.-G., et al. 2020, *RAA*, 20, 064
- Jiang, P., Yue, Y.L., Gan, H.Q., et al. 2019, *SCPMA*, 62, 1
- Koutsoloukas, L., Nikitas, N., & Aristidou, P. 2022, *Dev. Built Environ.*, 12, 100094
- Nagashima, I., & Shinozaki, Y. 1997, *EESD*, 26, 815
- Nan, R. 2006, *ScChG*, 49, 129
- Qian, L., Yao, R., Sun, J.H., et al. 2020, *Innov*, 1, 3
- Su, Y., Duan, B., Wei, Q., Nan, R., & Peng, B. 2003, *Mechatronics*, 13, 95
- Tang, X., Zhu, W., & S. C. Y. R. 2011, *ExA*, 29, 177